Structure-function relationship of the posterior subthalamic area with directional deep brain stimulation for essential tremor

Jean-Philippe Lévy [a,1], T.A. Khoa Nguyen [a,b,1], Lenard Lachenmayer [c], Ines Debove [c], Gerd Tinkhauser [c], Katrin Petermann [c], Alba Segura Amil [b], Joan Michelis [c], Michael Schüpbach [c], Andreas Nowacki [a,*], Claudio Pollo [a]

[a] Department of Neurosurgery, Inselspital, University Hospital Bern, University of Bern, Bern, Switzerland
[b] ARTORG Center for Biomedical Engineering Research, University of Bern, Bern, Switzerland
[c] Department of Neurology, Inselspital, University Hospital Bern, University of Bern, Bern, Switzerland

ARTICLE INFO

ABSTRACT

Deep Brain Stimulation of the posterior subthalamic area is an emergent target for the treatment of Essential Tremor. Due to the heterogeneous and complex anatomy of the posterior subthalamic area, it remains unclear which specific structures mediate tremor suppression and different side effects. The objective of the current work was to yield a better understanding of what anatomical structures mediate the different clinical effects observed during directional deep brain stimulation of that area.

We analysed a consecutive series of 12 essential tremor patients. Imaging analysis and systematic clinical testing performed 4–6 months postoperatively yielded location, clinical efficacy and corresponding therapeutic windows for 160 directional contacts. Overlap ratios between individual activation volumes and neighbouring thalamic and subthalamic nuclei as well as individual fiber tracts were calculated. Further, we generated stimulation heatmaps to assess the area of activity and structures stimulated during tremor suppression and occurrence of side effects.

Stimulation of the dentato-rubro-thalamic tract and the zona incerta was most consistently correlated with tremor suppression. Both individual and group analysis demonstrated a similar pattern of activation for tremor suppression and different sorts of side-effects. Unlike current clinical concepts, induction of spasms and paresthesia were not correlated with stimulation of the corticospinal tract and the medial lemniscus. Furthermore, we noticed a significant difference in the therapeutic window between the best and worst directional contacts. The best directional contacts did not provide significantly larger therapeutic windows than omnidirectional stimulation at the same level.

Deep brain stimulation of the posterior subthalamic area effectively suppresses all aspects of ET but can be associated with concomitant side effects limiting the therapeutic window. Activation patterns for tremor suppression and side effects were similar and predominantly involved the dentato-rubro-thalamic tract and the zona incerta. We found no different activation patterns between different types of side effects and no clear correlation between structure and function. Future studies with use of more sophisticated modelling of activation volumes taking into account fiber heterogeneity and orientation may eventually better delineate these different clusters, which may allow for a refined targeting and programming within this area.

1. Introduction

Essential tremor (ET) is a common movement disorder and affects about 4–5% of patients older than 65 years (Deuschl et al., 1998). In cases of severe tremor despite optimized medical treatment, deep brain stimulation is an effective and safe alternative (Limousin et al., 1999; Lozano, 2000). The ventral intermediate nucleus (VIM) of the thalamus is the classical and widely accepted target for DBS (Benabid et al., 1991;

Sammartino et al., 2016; Nowacki et al., 2018a). Alternatively, previous work has evaluated the efficacy of DBS in regions ventral to the thalamus that have been referred to as the zona incerta, the prelemniscal radiations, the posterior subthalamic area and the dentato-rubro-thalamic-tract by different groups (Carrillo-Ruiz et al., 2008; Blomstedt et al., 2010). A randomized, doubled blinded, crossover study compared the stimulation efficacy between DBS of the PSA versus VIM and found on average smaller effect thresholds in the PSA compared to the VIM (Barbe et al., 2018; Dembek et al., 2020). The diversity of names that have been used to describe these targets can be confusing but reflects the anatomical complexity of this region. The PSA is located ventral to the thalamus, lateral to the red nucleus and postero-medial to the sub-thalamic nucleus and contains the ZI as well as fiber tracts connecting the cerebellum and internal segment of the pallidum with the thalamus. These fiber tracts were historically considered as the prelemniscal radiations due to their anatomical position anterior to the sensory lemniscal pathway. An older view by Hassler describes the prelemniscal radiations as proprioceptive fibers from the medial lemniscus entering the VIM (Mai and Majtanik, 2019). More recently, anatomical and imaging analysis based on diffusion-weighted imaging identified the DRTT (or cerebello-thalamic tract) and pallidothalamic fibers as the two principal components of the prelemniscal radiations (Gallay et al., 2008; Coenen et al., 2011; Fiechter et al., 2017; Petersen et al., 2019).

Of note, different studies targeting the PSA yielded very good results with up to 80% tremor reduction despite the fact that the lead locations within the PSA varied considerably between and even within different groups (Kitagawa et al., 2000; Murata et al., 2003; Plaha et al., 2008; Fiechter et al., 2017). Previous studies analysed the possible role of the DRTT in mediating the tremor suppressive effect. Two previous studies found no correlation between tremor suppression and electrode distance to the tractography-based DRTT (Schlaier et al., 2015; Nowacki et al., 2018c). Another group found a positive, however statistically not significant correlation between electrode distance to the DRTT and tremor reduction (Coenen et al., 2014). The same group could later confirm this correlation statistically in a follow-up study of a bigger cohort (Coenen et al., 2020). None of the above cited studies provided a thorough investigation of stimulation-induced side effects, although the area's intricate anatomy with nearby structures and fiber tracts involved in diverse motor and sensory functions would implicate small therapeutic windows of stimulation. Thus, it is still a matter of debate which structure(s) mediate tremor suppression and which structures mediate different side effects within the PSA.

Segmented DBS leads have recently been developed and provide directional stimulation, which is spatially more confined than classical omnidirectional stimulation (Nguyen et al., 2019a). Thus, directional stimulation appears to be an optimal tool for a refined analysis of the structure-function relationship in the PSA. Based on modern imaging modalities including high-definition Q-ball imaging for tractography of different fiber tracts in combination with volume of tissue activated (VTA) modelling, the objective of the current work was to yield a better understanding of what anatomical structures mediate different clinical effects observed during DBS of the PSA. Furthermore, we wanted to assess if directional stimulation can activate more precisely tremor-suppressing structures, while avoiding those structures that mediate side effects.

2. Materials and methods

2.1. Patients

We analyzed a consecutive series of 12 patients (eight males) undergoing bilateral implantation of segmented DBS (Boston Cartesia Directional Leads) leads for treatment of refractory essential tremor between January 2016 and April 2018. Diagnosis of ET was assessed by specialized movement disorder neurologists according to recommended guidelines (Bhatia et al., 2018). Patients were discussed in a

multidisciplinary board prior to surgery. All patients provided written informed consent and the study was approved by the institutional review board (KEK 2018-00841).

2.2. Surgical planning and surgical procedure

Preoperative imaging was performed with a 3 T MRI system (MAGNETOM Trio Tim, Siemens) with patients under general anesthesia to reduce movement artifacts. A standard gadolinium-enhanced T1-weighted protocol (160 sagittal slices, 1 mm thickness) was followed by T2-weighted sequences (FOV 220 mm, acquisition matrix 128 × 128, TR 2000 ms, and multiple TE values ranging from 12 ms to 96 ms in steps of 12 ms). Diffusion-weighted echoplanar imaging was acquired with the following parameters: number of gradient directions 44, 2.2 mm slice thickness; 55 slices, TR 10,100 ms, TE 88 ms, field of view 280 mm, matrix 256 × 256, 1305 s/mm^2, overall voxel size 1.1 × 1.1 × 2.2 mm), b-values ranging from 1000 to 1305 with two b-0 images.

A preoperative high-resolution stereotactic CT scan was performed with the stereotactic frame in place (Leksell, Elekta). The target was defined visually on T2-weighted axial slices based on anatomical landmarks as described previously by our group (Nowacki et al., 2018a). Surgery was performed with the patient awake under local anesthesia with microelectrode guidance and intraoperative clinical testing. A postoperative high-resolution CT scan was performed the day after surgery for electrode reconstruction and to exclude early postoperative hemorrhage.

2.3. Clinical contact testing

Each patient underwent a systematic clinical assessment with monopolar stimulation of each contact at 4–6 months after DBS surgery under supervision of a specialized movement disorder neurologist during a short hospitalization on two consecutive days (day 1 ring-mode stimulation, day 2 testing of directional contacts). The examiner was blinded to the exact lead position and orientation. The examiner assessed resting, postural, action and intention tremor of all affected extremities. Symptom severity was rated clinically according to the Fahn-Tolosa-Marìn Tremor Clinical Rating Scale (Fahn et al., 1993). Stimulation frequency and pulse width were set to 130 Hz and 60 μs by default. Stimulation amplitude was increased stepwise in 0.5 mA increments starting at 1 mA. At each increment occurrence of dysarthria, twitching movements of upper and lower extremities and facial muscles, gaze and diplopia, ataxia (finger-to-finger and finger-to-nose test) and paraesthesia were tested and documented. The *effect threshold* was determined as the stimulation current necessary to achieve a first significant reduction of postural or action tremor (reduction of two points to moderate or discrete tremor). The side effect threshold was defined as the stimulation amplitude that provoked either a) significantly impairing dysarthria, b) muscle spasms or twitching of either facial muscles or in the extremities, c) sustained paraesthesia, d) diplopia, e) oscillopsia or f) significant ataxia. We regrouped diplopia and oscillopsia under oculomotor side effects. We defined the therapeutic window as the difference between side effect and effect thresholds.

2.4. Diffusion-weighted imaging analysis and tractography

The local fiber orientation distribution was estimated from Q-ball imaging, which approximates a local fiber orientation distribution function by applying the Funk-Radon-Transform on a spherical acquisition scheme (Tuch et al., 2003; Tuch, 2004). Fiber tracking was performed with DSI Studio (version June 2018) to display the medial lemniscus, the corticospinal tract as well as the dentato-rubro-thalamic tract. To this end, the diffusion data were reconstructed using generalized q-sampling imaging (Yeh et al., 2010) with a diffusion sampling length ratio of 1.25. The restricted diffusion was quantified using restricted diffusion imaging (Yeh et al., 2017). For the CST, the pre-

central gyrus and the posterior limb of the internal capsule were set as regions of interest (ROIs) and the cerebral peduncle as seed. For the DRTT, the dentate nucleus and precentral gyrus were set as ROIs and the thalamus as seed. For the ML, the post-central gyrus and thalamus were set as ROIs and a manually segmented region posterior to the midbrain as seed as described previously (Nowacki et al., 2018c).

In generalized q-sampling imaging, the anisotropy threshold used for fiber termination is based on the quantitative anisotropy (QA), which is defined for each resolved fiber orientation. The initial value of this threshold is determined automatically using 0.6 * (Otsu's threshold). Otsu's method calculates the optimal separation threshold that maximizes the variance between the background and foreground (Yeh et al., 2010). The anisotropy threshold used was the QA value defined by default. The maximum turning angle for terminating the tracking if two consecutive moving directions had a crossing angle above this threshold was 60°. The step size defining the moving distance in each tracking interval was the default value set as half of the spatial resolution, 1.1 mm. A minimum length of 10 mm and a maximum length of 300 mm were used to obtain the tracts of interest.

2.5. Lead reconstruction and estimation of volume of tissue activated

Lead reconstruction and volume of tissue activated modelling was performed with the Lead-DBS toolbox (version 2.2.3) in Matlab 2016b (The Mathworks, Natick, MA, USA) as described recently by our and other groups (Nowacki et al., 2018b; Horn et al., 2019; Nguyen et al., 2019b). Image sets were co-registered and normalized into the MNI space (MNI ICMB 2009b) using Statistical Parametric Mapping 12 and Advanced Normalization Tools (Avants et al., 2008). A brainshift correction was applied with the coarse and fine mask (Schönecker et al., 2009; Horn et al., 2019). Each co-registration and normalization were checked manually before further processing. The electrode trajectory and position were reconstructed semi-automatically using PaCER and corrected manually if judged necessary (Husch et al., 2018; Nowacki et al., 2018b). The VTA was calculated using the SimBio/Field Trip algorithms (Oostenveld et al., 2011; Vorwerk et al., 2018) with default parameters for conductivities and threshold in Lead-DBS.

Lead orientation was assessed using anterior-posterior and lateral skull X-rays performed three to five days following implantation. The marker on the Boston Cartesia directional lead was used to determine its orientation, in estimated 45°-steps (anterior, anteromedial/anterolateral, medial/lateral, posteromedial/posterolateral and posterior). The automatic detection of the lead orientation in Lead DBS (version 2.3.2, Hellerbach et al., 2018) was not successful as our surgical approach yielded large polar angles. This resulted in hardly visible streak artifacts of the marker, which the automatic detection relies upon.

2.6. Atlas construction

Anatomical structures of the PSA were displayed in MNI space based on previously published three-dimensional human brain atlases. Thalamic nuclei were named according to the adapted nomenclature of Hirai and Jones (Macchi and Jones, 1997). Specifically, we imported a) the Red Nucleus, the Subthalamic nucleus, the ventral lateral anterior nucleus, the ventral and dorsal part of the ventral lateral posterior nucleus from the Morel atlas of the human thalamus (Krauth et al., 2010); b) the Zona incerta from the DISTAL atlas (Ewert et al., 2018); c) the corticospinal tract, the medial lemniscus, the dentato-rubro-thalamic tract from our patient's cohort as described above. For the overlap ratio analysis we grouped VLa, VLpv, VLpd as the motor thalamus (VL) for the sake of clarity.

2.7. VTA analysis

To gain a better understanding of the PSA and what anatomical structures mediate different clinical effects, we divided the analysis into two parts. In the first part, we were interested identifying the *minimal set* or origin of structures that mediate a certain effect. To this end, we specifically selected certain stimulation settings from each lead further detailed below. In the second part, we were interested in an overview of the PSA and the spatial distribution of stimulation clusters. To that end, we included *all* stimulation settings from each lead. These were used to compute mean effect and significant mean effect images (Dembek et al., 2017, 2019; Nguyen et al., 2019b).

In the first part, for each lead VTAs were calculated for the contact with the lowest effect threshold as well as the contacts with the lowest threshold to induce any of the above listed side effects where applicable. In cases where two or more electrode contacts per lead induced tremor suppression or a given side effect at the same amplitude, each corresponding VTA was calculated and included in the final analysis. We did not include VTAs corresponding to side effects that were elicited at higher amplitudes to better identify the origin of an effect (i.e., if in patient 1 on contact 2 and 4 dysarthria was induced at 3.5 mA and on contact 5 at 4.0 mA, only the corresponding VTAs of contact 2 and 4 were included in the analysis). We determined the overlap ratio between individual VTAs and the atlas- and tractography-based anatomical structures of interest (Nguyen et al., 2019b).

The overlap ratio provides a quantitative measure, which critically depends on the size of the structure of interest (complete overlap of a given VTA with a small structure such as the DRTT will ultimately lead to a small overlap ratio). Therefore, we have focused our results on the qualitative structure-function analysis, assessing if a structure was (partially) covered (overlap-ratio > 0) by a given VTA or not.

In the second part, we computed effect and significant mean effect images for tremor suppression and side effects, similar to previous work (Dembek et al., 2017, 2019; Nguyen et al., 2019b). We estimated VTAs at effect and side effect thresholds for *each contact*. Of note, a contact can have only one effect VTA but several side effect VTAs, if the activation of that contact evoked different side effects. Then, we computed separate mean effect images for tremor suppression, dysarthria, paresthesia, dystonia and spasm. The voxels of each VTA were assigned a score of 1/current amplitude. Afterwards, the mean effect images underwent voxelwise statistical testing to determine significant mean effect images. For tremor suppression, we set an alpha level of 0.05 and added type I error correction with a false discovery rate (Genovese et al., 2002). For side effects, mean effect images did not pass type I error correction due to smaller sample size. Instead we applied an alpha level of 0.001. These significant mean effect images are therefore probably overestimated (significant mean effect images are available as supplementary MATLAB fig files). Finally, we extracted a cluster from each image by selecting those 10% voxels with the highest scores.

2.8. Therapeutic windows

For therapeutic window analysis, we adapted the method reported by Steigerwald et al. 2016 (Steigerwald et al., 2016). We calculated the therapeutic window (therapeutic window (mA) = side effect threshold (mA) − effect threshold (mA)) of each directional contact and the corresponding (omnidirectional) ring-level. At each level, we compared the therapeutic windows of the best and worst directional contacts against the therapeutic window of the ring level. Effect threshold was defined as the stimulation amplitude at which a first significant reduction in action or postural tremor occurred.

2.9. Statistical analysis

Descriptive statistics and statistical testing were performed with GraphPad Prism 8.

For the quantitative structure-function analysis we determined the normalized overlaps for each structure and the observed clinical effect as the number of times a given structure was (partially) covered by the VTA corresponding to the observed clinical effect per total number of

times the given clinical effect was elicited. A correlation matrix was calculated to test for similarities between different clinical effects and their activation patterns of associated structures using Spearman's correlation with a two-sided p-value and a 95%-confidence interval. Stimulation profiles of each clinical effect were visualized by heatmaps of the normalized overlaps. Data is provided as mean ± standard deviation if not otherwise indicated. The statistical significance level was set at P < 0.05.

2.10. Data availability statement

Raw data were generated at the University Hospital Bern. Derived data supporting the findings of this study are available from the corresponding author on request.

3. Results

3.1. Patient demographics, electrode placement and VTA calculation

Ten patients were included in the final analysis. Two patients had to be excluded. In one patient the diagnosis was adapted in the course of the study to Parkinson's disease and in the second patient MR imaging data was of insufficient quality to be analyzed. Mean patient age was 63 ± 13 years.

All leads were placed within the PSA with a homogenous distribution along its anterior-posterior axis (Fig. 1).

3.2. Clinical effects during PSA stimulation

The mean effect threshold for postural tremor suppression was 1.97 ± 0.84 mA. We could suppress all aspects of tremor (action, postural, intention) in 19 out of 20 hemispheres at usually higher amplitudes

Fig. 1. Lateral (A), anterior (B) and posterior (C) view of all examined electrodes (*blue*: STN, *red*: RN, *yellow*: ZI, *orange*: DRTT). (For interpretation of the references to colour in this figure legend, the reader is referred to the web version of this article.)

(2.67 ± 0.76 mA). Spasms were the most frequently observed side effects (n = 27) with a mean threshold of 2.96 ± 0.66 mA. Dysarthria (n = 16), oculomotor side effects (n = 15), ataxia-dysmetria (n = 11), and paresthesia (n = 9) were observed less frequently. The mean threshold for occurrence of these side effects were 2.66 ± 0.89 mA (dysarthria), 4.0 ± 1.1 mA (oculomotor side effects), 3.14 ± 0.95 mA (ataxia), 2.83 ± 1.25 mA (paresthesia), respectively.

3.3. VTA analysis

In the first part of our analysis, we calculated the VTAs according to the stimulation settings that induced effects and different side effects at the lowest threshold for a given lead.

For tremor suppression, the structures most frequently activated by corresponding VTAs were the ZI (n = 34) and DRTT (n = 30) followed by STN (n = 20) and RN (n = 17). The motor thalamus (VL) was only covered by five VTAs. Even less frequently, VTAs covered the CST (n = 2) and ML (n = 1). A similar pattern of activation was found for different side effects (Fig. 2). Of note, VTAs that were associated with induction of spasms covered the CST in only 2 cases and VTAs that were associated with occurrence of paresthesia did not cover the ML in any of the cases. Overlap ratios are compiled in Supplementary Table 1.

The second part of our analysis revealed tightly placed clusters within the PSA (Fig. 3). The cluster for tremor suppression extended more dorsal and lateral towards the ZI compared to clusters of dystonia, spasm and dysarthria that were located more medially and caudally. Of note, the clusters for spasms was located centrally within the PSA and distant to the reconstructed fiber tracts of the CST and ML.

3.4. Influence of directional stimulation on therapeutic windows

The median therapeutic window across all directional and omnidirectional contacts was 1 mA. To investigate the influence of directional stimulation, we compared the therapeutic windows of best and worst directional contacts with the window of their corresponding ring level stimulation. At the most effective level, the therapeutic window of the best directional contacts was not significantly different from the therapeutic window of the ring level. However, the worst directional contact had a significantly (p < 0.01) smaller therapeutic window compared to ring-mode stimulation (Fig. 4). There was a statistically significant difference between the therapeutic windows of the most effective and least effective contact at each ring level (p < 0.01).

4. Discussion

To the best of our knowledge, the current work is the first in-depth analysis of stimulation-induced effects of directional DBS of the PSA focusing not only on tremor-suppression but also elicitation thresholds of different clinically relevant side-effects. Our study highlights some key findings. First, stimulation of the PSA completely suppressed all aspects of essential tremor in 19 out of 20 hemispheres. Second, limiting stimulation-induced side effects are common in this region and lead to narrow therapeutic windows of on average 1 mA. The most frequent side effects we observed were spasms (n = 27), dysarthria (n = 16) and oculomotor side effects (n = 15). Third, the narrow therapeutic windows are reflected by tightly placed and largely overlapping clusters for tremor suppression and elicitation of different sorts of side-effects. Specifically, both tremor reduction and induction of side-effects were correlated with activation of the same structures comprising the ZI, DRTT, STN and RN. Surprisingly, induction of muscle spasms and paraesthesias were not associated with activation of the CST and ML, a finding with implications on the classical concepts of "capsular" and "lemniscal" side-effects. Finally, directional stimulation had a small impact on the therapeutic window. The therapeutic windows were significantly different for the best and worst directional contacts, whereas the best directional contacts did not provide a significantly
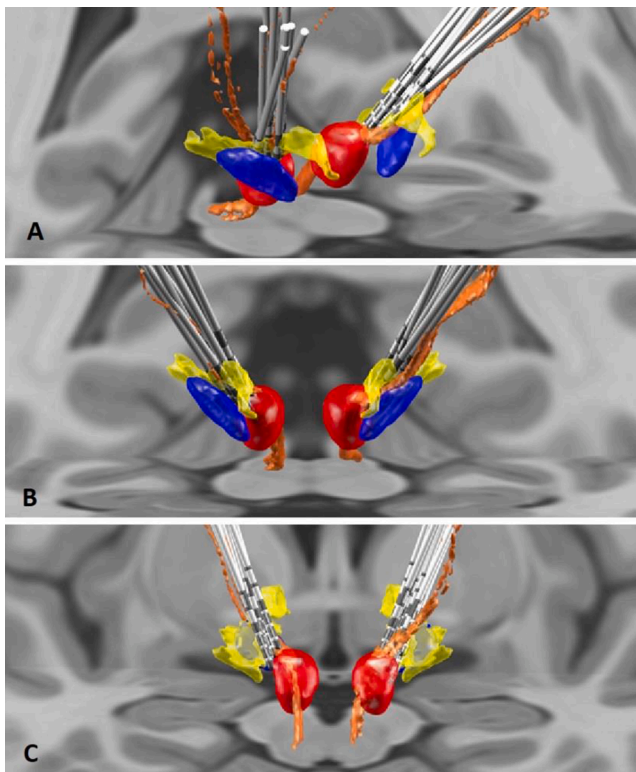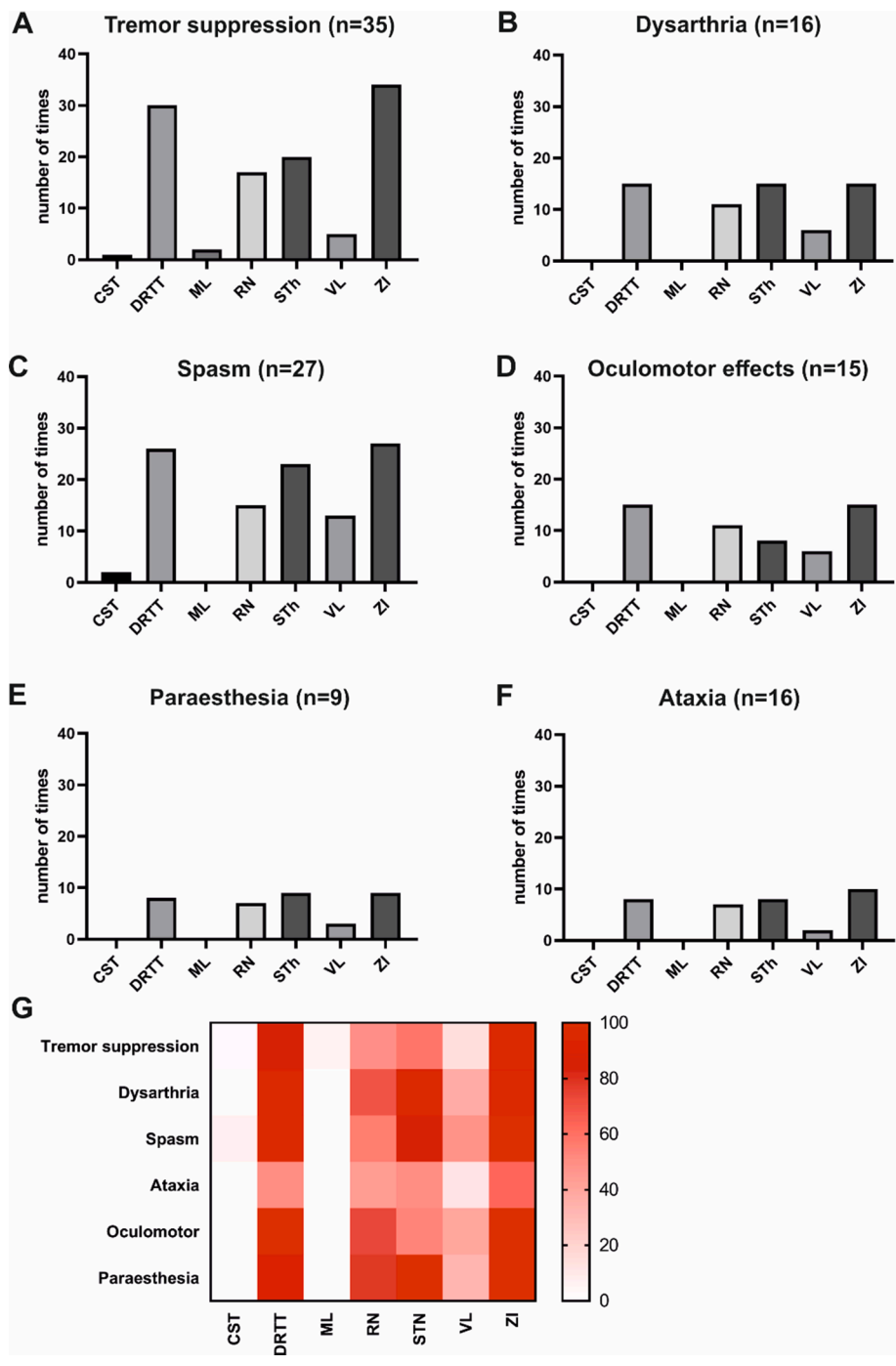
Fig. 2. Quantitative analysis of the overlap ratios regarding tremor reduction (A; CST: 1, DRTT: 30, ML: 2, RN: 17, STN: 20, VL: 5, ZI: 34), dysarthria (B; CST: 0, DRTT: 15, ML: 0, RN: 11, STN: 15, VL: 6, ZI: 15), spasm (C; CST: 2, DRTT: 26, ML: 0, RN: 15, STN: 23, VL: 13, ZI: 27), oculomotor side effects (D; CST: 0, DRTT: 15, ML: 0, RN: 11, STN: 8, VL: 6, ZI: 15), paresthesia (E; CST: 0, DRTT: 8, ML: 0, RN: 7, STN: 9, VL: 3, ZI: 9) and ataxia (F; CST: 0, DRTT: 8, ML: 0, RN: 7, STN: 8, VL: 2, ZI: 10). G: Heat map: TR vs Dysarthria (R 0.9543, $p < 0.05$), TR vs Spam (R 0.9643, $p < 0.05$), TR vs Ataxia and Dysmetria (R 0.9820, $p < 0.05$), TR vs Oculomotor side effects (R 0.9456, $p < 0.05$), TR vs Paresthesia (R 0.9274, $p < 0.05$). The clusters for oculomotor side effects and ataxia are not included for the sake of clarity.

larger window than omnidirectional stimulation at that level.

4.1. Anatomical considerations

The PSA is an intricate and inhomogeneous region that is located inferior to the ventral thalamus. It is difficult to give an exact anatomical definition of the PSA. According to Blomstedt the clockwise anterior, lateral, posterior and medial border of the PSA are the posterior border of the STN, the posterior limb of the internal capsule, the medial lemniscus and the red nucleus (Blomstedt et al., 2009). Especially the anterior border is ill-defined on human brain atlases and constitutes the pallidothalamic fiber tracts (consisting of the fasciculus lenticularis and ansa lenticularis) that have been classically referred to as the Fields of Forel 1 and 2. The main principal components of the PSA are the zona incerta and the prelemniscal radiations. More recent work has refined our understanding of the prelemniscal radiations, which is composed primarily of cerebellothalamic fibers (also known as the dentate-rubro-thalamic tract, DRTT) as well as fibers originating from the mesencephalic reticular formation (Gallay et al., 2008). The zona incerta is regarded as the rostral continuation of the brain stem reticular formation and is composed of loosely arranged cell groups. Based on extensive connections with the brainstem reticular formation including the pedunculopontine nucleus and parabrachial nucleus, the red nucleus, superior colliculus, cerebellar nuclei, basal ganglia as well as thalamus, cerebral cortex, and spinal cord, it is regarded as an important hub within both the thalamocortico-basal ganglia and the cerebello-thalamocortical circuits (Kolmac et al., 1998; Mitrofanis and Mikuletic, 1999; Power et al., 1999; Blomstedt et al., 2009).
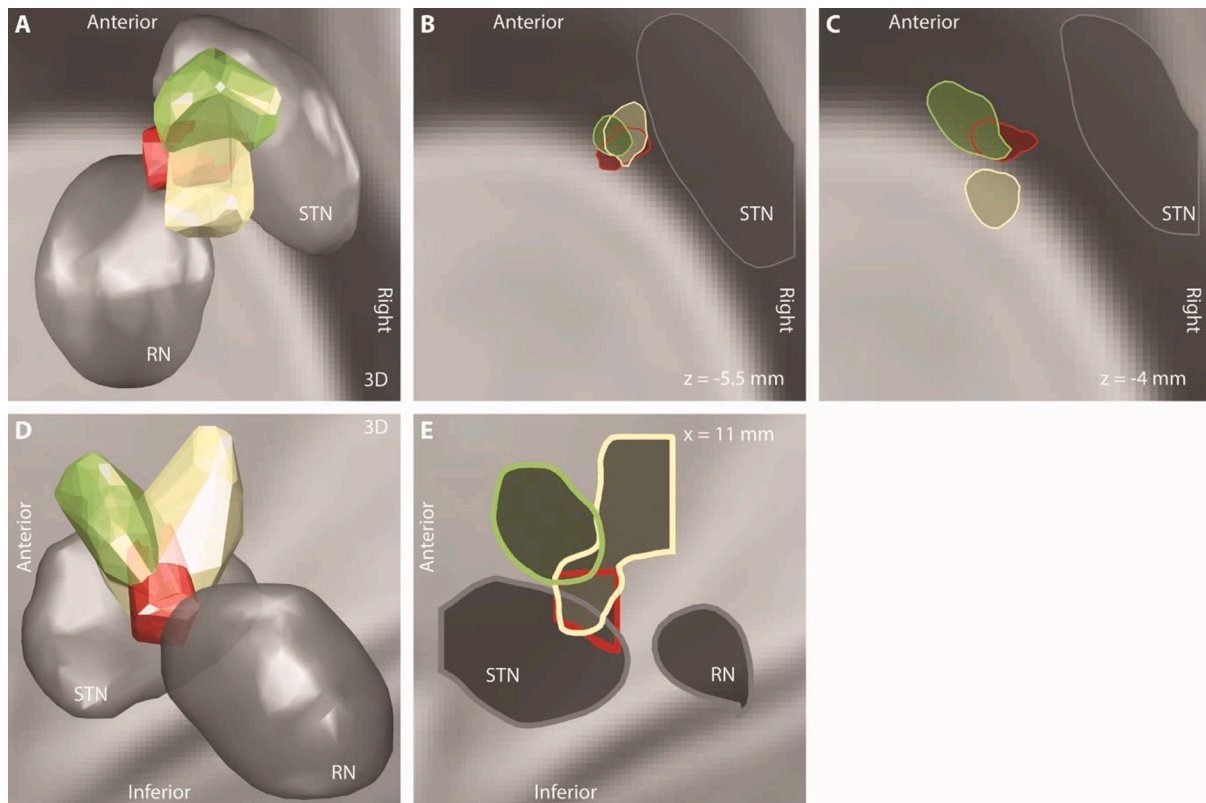
Fig. 3. A)-E) Axial and sagittal views of effect and side effect clusters as well as subthalamic nucleus (STN) and red nucleus (RN). A) and D) are pseudo-3D views of the clusters and illustrate the overlap between them. Green cluster denotes tremor suppression, red cluster dysarthria, orange cluster paresthesia, yellow cluster dystonia and spasm. B) and C) show axial sections of the clusters and subthalamic nucleus at z = -5.5 mm and −4 mm, respectively (MNI coordinate system). E) shows a sagittal section at x = 11 mm. (For interpretation of the references to colour in this figure legend, the reader is referred to the web version of this article.)
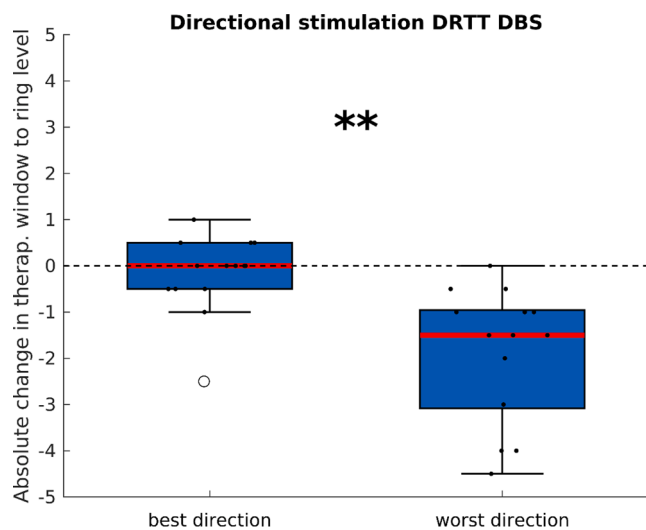

Fig. 4. Box plot comparing the therapeutic windows between best and worst directional contacts on the most effective level. Left: absolute difference in therapeutic window between best directional contact and ring level. The median difference was 0 mA and not significant. Right: absolute difference in therapeutic window between worst directional contact and ring level (median difference −1.5 mA, p < 0.01). There was also a significant difference between best and worst directional contact (median difference −1.5 mA, p < 0.01).

4.2. Functional considerations of tremor suppression

The arising question, which structure(s) mediate(s) the tremor-suppressive effect or side effects of PSA-DBS has been addressed before (Plaha et al., 2008; Blomstedt et al., 2010, 2011; Coenen et al., 2014, 2020). The ZI quickly became a suggested target to control tremor of various pathologies (ET, Parkinson's disease, multiple sclerosis, dystonic tremor) by some groups (Plaha et al., 2008; Coenen et al., 2014, 2020) while our previous work as well as work of other groups have pointed towards the DRTT as the common structure (Coenen et al., 2014, 2020; Fiechter et al., 2017). Moreover, a recent study showed that tremor suppression efficacy directly depends on the distance to the DRTT (Dembek et al., 2020). These studies explored the structure-function relationship with omnidirectional leads (Fytagoridis et al., 2013; Dembek et al., 2017), whereas the present study is based on segmented leads that provide a spatially more confined directional stimulation. Our current findings support both previous hypotheses that both the DRTT and ZI are involved in tremor suppression. Furthermore, in a relevant number of patients we demonstrate a co-stimulation of the STN and RN. There are at least two possible underlying mechanisms of this finding. Either, tremor suppression might be mediated by stimulation of a certain compartment of one structure – the DRTT or the ZI – and coverage of this compartment by the stimulation field inevitably leads to co-stimulation of nearby structures. Or, effective tremor suppression requires co-stimulation of the DRTT and the ZI. Current limitations of the applied technology do not permit a definitive answer at this point.

4.3. Functional considerations of side-effects

Previous studies in the field of DBS for tremor in the PSA have mainly reported clinical outcome for tremor suppression but few studies have reported a detailed analysis of side-effects (Kitagawa et al., 2000; Murata et al., 2003; Plaha et al., 2008; Fiechter et al., 2017; Coenen et al., 2020). However, stimulation-induced side effects have been a major limiting factor of DBS for ET in clinical practice and a thorough

understanding of the structure-function relationship of stimulation-induced side-effects is warranted to help anticipate and avoid these effects with the help of modern current steering technology. To our knowledge only two previous studies analyzed the structure-function-relationship of different side-effects in detail. Fytagoridis et al. analyzed DBS electrode locations within the PSA of 33 hemispheres regarding stimulation-induced side effects (Fytagoridis et al., 2013). Similar to our findings, paresthesia and muscle contractions or cerebellar signs could not be attributed to a certain structure or anatomical region within the PSA. Unlike the present work, Fytagoridis' analysis was based on omnidirectional stimulation, without VTA modelling and normalization of datasets into a common template space such as the MNI space but plotted electrode locations onto the 2-D stereotactic atlas of Morel. More recently, Dembek et al. analyzed stimulation sites and stimulation effects of 16 ET patients targeted at the VIM region by probabilistic mapping in the MNI space using VTA modelling (Dembek et al., 2017). The authors assessed reduction of postural and intention tremor as well as occurrence of dysarthria, paraesthesia and dizziness. Interestingly, the highest likelihood of tremor reduction was found in ventrally located regions of the thalamus and the posterior subthalamic area. In line with our results, different sorts of side-effects were not associated with stimulation of one specific but several structures. For instance, induction paraesthesia was correlated with a stimulation field covering large parts of the Vim, ZI, CM and VPI/VPM/VPL. The authors did not report on the side-effect thresholds and therapeutic windows that our present results could be compared to.

Thus, our findings agree with previous work and underline some interesting and unexpected findings: we found a similar activation pattern for both tremor suppression and induction of different side-effects. Regardless of what clinical effect we observed, the structures that were most frequently stimulated were the ZI, DRTT, RN and STN. Our heatmap analysis confirmed tight and overlapping clusters of side effects in the center of the PSA. Of note, induction of paresthesia was not

associated with stimulation of the ML and induction of muscle spasms were associated with CST activation in only a vast minority of the patients. These findings are against current concepts presented in most textbooks that refer muscle spasms and contractions to as "capsular" side effects and paresthesias as "lemniscal" side effects. There are several possible explanations for our findings. First, current imaging technologies are limiting. For example, diffusion-weighted imaging and tractography algorithms (for display of fiber tracts such as the ML, CST and DRTT) as well as current VTA models that are based on simplified assumptions (such as exclusive axonal activation with fixed electrical properties and orientation towards the electrode, ignorance of field inhomogeneities and anisotropy) may not be accurate enough to display activation of the structures of interest in the anatomically intricate PSA (Fig. 5a and b). Accordingly, paresthesias and spasms are mediated by current spread to the ML and CST, but this activation is not captured by the VTA model. Second, different side effects such as paresthesia or muscle contractions/spasms are indeed not induced by direct activation of the CST or ML but reflect phenomena based on the network properties of the cerebello- and basal ganglia-thalamocortical loops (Fig. 5c).

4.4. Clinical implications

This study confirms previous findings by other groups that the PSA is an effective area for tremor suppression. However, limiting therapeutic side-effects are common and lead to overall small therapeutic windows. In a complex area such as the PSA, directional stimulation may improve the therapeutic window as demonstrated in STN DBS for Parkinson's disease (Steigerwald et al., 2016). For essential tremor, this has been recently shown for directional DBS of the Vim (Rebelo et al., 2018). The Oxford group could demonstrate significant gains in the therapeutic window and reductions in current consumption with stimulation in the best direction compared to best omnidirectional stimulation alternative (Meidahl et al., 2017). We also observed significant differences in
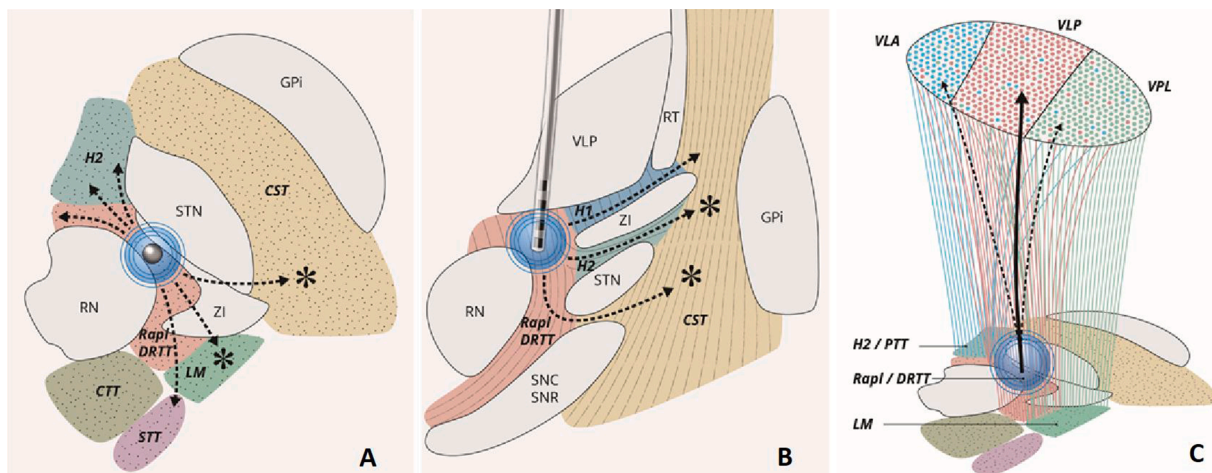

Fig. 5. Schematic axial (a) and horizontal (b) drawings of the PSA. The drawings represent the estimated volume of tissue activated (VTA) by current modelling technology that covers the Rapl/DRTT, zona incerta (Zi), subthalamic nucleus (STN) and red nucleus (RN). Due to limitations of the underlying model assumptions current spread along pathways of low tissue conductance (arrows) are not captured that, in reality, might exist and activate (stars) structures like the CST and ML which in turn induce spasms and paresthesias. (c) In this alternative explanation, the stimulation field (blue circle) leads to pure activation of the Rapl/DRTT and the ZI. Activation of affected fibers could result in the observed side-effects (paraesthesias, spasms, dysarthria, oculomotor or ataxia) by modulating thalamic or thalamo-cortical signal processing. Anatomical studies have demonstrated efferent connections of both the cerebellar nuclei (via the Rapl/DRTT) and ZI to the ventral posterior (sensory) thalamus (indicated by red fibers terminating in VPL) which is predominantly targeted by the medial lemniscus (LM) (Sakai et al., 1996; Power et al., 1999). Thus activation of the DRTT could induce paraesthesia by cross-activation of the VPL. Apart from the main projections to the posterior part of the Ventral lateral nucleus (VLP), the DRTT further targets the anterior part of the VL (VLA) which predominantly receives input from the internal pallidal segment (blue fibers running through H2) which could induce dysarthria (Sakai et al., 1996). Furthermore, there is evidence for intrathalamic interactions between modality-specific regions in the dorsal thalamus as a potential crosslink between parallel motor, sensory and affective channels (John W. Crabtree et al., 1998). Thus, the thalamic relay nuclei integrate both lemniscal, cerebellar and pallidal inputs and it is possible that stimulation of one input structure influences signal processing of the other, thereby inducing the clinical motor side-effects. Furthermore, there are connections between the ZI and the superior colliculus, the cerebellar nuclei and multiple brain stem nuclei modulation of which could account for the observed side-effects (Kolmac et al., 1998). (For interpretation of the references to colour in this figure legend, the reader is referred to the web version of this article.)

therapeutic window between best and worst directional stimulation. Although best directional stimulation tended to have larger therapeutic windows than omnidirectional stimulation, the differences were not significant. This is likely due to the tight clusters that allow only minimal space to maneuver directional stimulation. Additionally, the small differences in the therapeutic window between directional and omnidirectional stimulation could be based on the rather consistent location of our electrodes in the center of the PSA. The anatomical complexity of the target structure and co-stimulation of surrounding fiber tracts, the nearby ZI, STN and RN even with low amplitudes might explain the small differences in the therapeutic windows between directional and omnidirectional stimulation. In contrast to our findings, a recent study by Bruno and co-workers found a small but significant difference between omnidirectional and directional stimulation of the VIM and PSA. (Bruno et al., 2020). Therefore, whether PSA stimulation may ultimately benefit from directional current steering would need to be explored in additional studies.

We did not evaluate the role of different stimulation pulse widths on the therapeutic window. Recent computational models found that long pulse widths might focus the stimulation effect on small, nearby fibers, thereby suppressing distant white matter tract activation which can be responsible for some DBS side-effect (Anderson et al., 2020). This concept seems interesting, especially in an anatomically heterogeneous area such as the PSA, which comprises many fiber tracts with probably different electrophysiological properties. This hypothesis needs to be tested in future studies.

5. Limitations

Our study has several limitations. Our cohort consisted of a small number of patients, which restricts the statistical robustness of our work. Of note, most other studies were conducted with a similar number of patients. Secondly, we used a VTA model that does not take into account field inhomogeneities and field anisotropy as well as the varying electrical properties of different fiber tracts present in the PSA. A more sophisticated VTA model that incorporates activation models of more than just one axon-type and that takes into account field inhomogeneities would be warranted. Moreover, our algorithm dedicated to co-registration and normalization comes along with inherent errors and impacts the overall accuracy of the model. The selection for the appropriate atlas available in MNI space merits a further point of discussion. Of note, the definition of the ZI remains elusive. Due to the reticular character of this nucleus, there are no clear-cut boundaries and a precise definition and delineation for their structure remains controversial. To integrate all structures of interest in our analysis, we had to combine two different atlases and in-house-Q-ball imaging-based tractography to delineate the fiber tracts. This patch-work could also contribute to some inaccuracies of the model. Furthermore, our mapping was performed with steps of 0.5 mA in our clinical routine which may decrease the specificity and accuracy of positive and side effects in the therapeutic window analysis. Lastly, the lead orientation was assessed three to five days postoperatively based to skull radiographs. Thus, there remains some uncertainty about the exact electrode orientation in the range of 10° which has further implications on model accuracy. We cannot exclude an additional rotation of the lead between the postoperative X-rays and the time of clinical testing, through this is probably unlikely. More recent methods allow for the detection of the lead orientation (Reinacher et al., 2017; Horn et al., 2019; Steigerwald et al., 2019). Due to the low intensity profile of the electrode orientation marker on our postoperative CT sequences and the resulting flat similarity indices, we could not run the automatic orientation detection implemented in LEAD 2.3.2 (Hellerbach et al., 2018).

6. Conclusions

In summary, we aimed at gaining a better understanding of what anatomical structures mediate different clinical effects observed during DBS of the PSA. We found similar activation patterns and clusters for effect and side effects based on directional stimulation. Tremor suppression is most likely mediated by activation of the DRTT and ZI and current technology does not provide a clear structure-function relationship of different observed side effects. We suggest that future studies need to apply VTA-models that are more sophisticated and focus on the role of different stimulus pulse widths to work out differences between the obviously very tightly located clusters of effect and different side effects. This might eventually lead to an even better understanding of the different compartments of the PSA with implications on targeting approaches and current-steering technologies to fully exploit the potential of DBS in this area.

CRediT authorship contribution statement

Jean-Philippe Lévy: Methodology, Formal analysis, Investigation, Writing - original draft. **T.A. Khoa Nguyen:** Methodology, Software, Validation, Formal analysis. **Lenard Lachenmayer:** Resources. **Ines Debove:** Resources. **Gerd Tinkhauser:** Methodology, Resources. **Katrin Petermann:** Resources. **Alba Segura Amil:** Methodology, Formal analysis. **Joan Michelis:** Resources. **Michael Schüpbach:** Resources. **Andreas Nowacki:** Conceptualization, Formal analysis, Project administration. **Claudio Pollo:** Project administration, Supervision.

Declaration of Competing Interest

The authors declare that they have no known competing financial interests or personal relationships that could have appeared to influence the work reported in this paper.

Appendix A. Supplementary data

Supplementary data to this article can be found online at https://doi.org/10.1016/j.nicl.2020.102486.

References

Anderson, C.J., Anderson, D.N., Pulst, S.M., Butson, C.R., Dorval, A.D., 2020. Neural selectivity, efficiency, and dose equivalence in deep brain stimulation through pulse width tuning and segmented electrodes. Brain Stimul. https://doi.org/10.1016/j.brs.2020.03.017.

Avants, B.B., Epstein, C.L., Grossman, M., Gee, J.C., 2008. Symmetric diffeomorphic image registration with cross-correlation: evaluating automated labeling of elderly and neurodegenerative brain. Med. Image Anal. 12, 26–41. https://doi.org/10.1016/j.media.2007.06.004.

Barbe, M.T., Reker, P., Hamacher, S., Franklin, J., Kraus, D., Dembek, T.A., Becker, J., Steffen, J.K., Allert, N., Wirths, J., Dafsari, H.S., Voges, J., Fink, G.R., Visser-Vandewalle, V., Timmermann, L., 2018. DBS of the PSA and the VIM in essential tremor: a randomized, double-blind, crossover trial. Neurology 91, e543–e550. https://doi.org/10.1212/WNL.0000000000005956.

Benabid, A.L., Pollak, P., Hoffmann, D., Gervason, C., Hommel, M., Perret, J.E., de Rougemont, J., Gao, D.M., 1991. Long-term suppression of tremor by chronic stimulation of the ventral intermediate thalamic nucleus. Lancet 337, 403–406. https://doi.org/10.1016/0140-6736(91)91175-T.

Bhatia, K.P., Bain, P., Bajaj, N., Elble, R.J., Hallett, M., Louis, E.D., Raethjen, J., Stamelou, M., Testa, C.M., Deuschl, G., 2018. Consensus Statement on the classification of tremors from the task force on tremor of the International Parkinson and Movement Disorder Society. Movement Disorders 33, 75–87. https://doi.org/10.1002/mds.27121.

Blomstedt, P., Sandvik, U., Fytagoridis, A., Tisch, S., 2009. The posterior subthalamic area in the treatment of movement disorders: past, present, and future. Neurosurgery 64, 1029–1038. https://doi.org/10.1227/01.NEU.0000345643.69486.BC discussion 1038–42.

Blomstedt, P., Sandvik, U., Tisch, S., 2010. Deep brain stimulation in the posterior subthalamic area in the treatment of essential tremor. Movement Disorders 25, 1350–1356. https://doi.org/10.1002/mds.22758.

Blomstedt, P., Sandvik, U., Linder, J., Fredricks, A., Forsgren, L., Hariz, M.I., 2011. Deep brain stimulation of the subthalamic nucleus versus the zona incerta in the treatment of essential tremor. Acta Neurochir. 153, 2329–2335. https://doi.org/10.1007/s00701-011-1157-4.

Bruno, S., Nikolov, P., Hartmann, C.J., Trenado, C., Slotty, P.J., Vesper, J., Schnitzler, A., Groiss, S.J., 2020. Directional deep brain stimulation of the thalamic ventral

intermediate area for essential tremor increases therapeutic window. Neuromodulation. https://doi.org/10.1111/ner.13234.

Carrillo-Ruiz, J.D., Velasco, F., Jimènez, F., Castro, G., Velasco, A.L., Hernández, J.A., Ceballos, J., Velasco, M., 2008. Bilateral electrical stimulation of prelemniscal radiations in the treatment of advanced Parkinson's disease. Neurosurgery 62, 347-57; discussion 357-9. DOI:10.1227/01.neu.0000316001.03765.e8.

Coenen, V.A., Allert, N., Mädler, B., 2011. A role of diffusion tensor imaging fiber tracking in deep brain stimulation surgery: DBS of the dentato-rubro-thalamic tract (drt) for the treatment of therapy-refractory tremor. Acta Neurochir. 153, 1579–1585. https://doi.org/10.1007/s00701-011-1036-z discussion 1585.

Coenen, V.A., Allert, N., Paus, S., Kronenbürger, M., Urbach, H., Mädler, B., 2014. Modulation of the cerebello-thalamo-cortical network in thalamic deep brain stimulation for tremor: a diffusion tensor imaging study. Neurosurgery 75, 657-69; discussion 669-70. DOI:10.1227/NEU.0000000000000540.

Coenen, V.A., Sajonz, B., Prokop, T., Reisert, M., Piroth, T., Urbach, H., Jenkner, C., Reinacher, P.C., 2020. The dentato-rubro-thalamic tract as the potential common deep brain stimulation target for tremor of various origin: an observational case series. Acta Neurochir. https://doi.org/10.1007/s00701-020-04248-2.

Crabtree, John W., Collingridge, Graham L., Isaac, John T.R., 1998. A new intrathalamic pathway linking modality-related nuclei in the dorsal thalamus. Nat. Neurosci. 1, 389–394. https://doi.org/10.1038/1603.

Dembek, T.A., Barbe, M.T., Åström, M., Hoevels, M., Visser-Vandewalle, V., Fink, G.R., Timmermann, L., 2017. Probabilistic mapping of deep brain stimulation effects in essential tremor. NeuroImage Clin. 13, 164–173. https://doi.org/10.1016/j.nicl.2016.11.019.

Dembek, T.A., Hoevels, M., Hellerbach, A., Horn, A., Petry-Schmelzer, J.N., Borggrefe, J., Wirths, J., Dafsari, H.S., Barbe, M.T., Visser-Vandewalle, V., Treuer, H., 2019. Directional DBS leads show large deviations from their intended implantation orientation. Parkinsonism Related Disorders 67, 117–121. https://doi.org/10.1016/j.parkreldis.2019.08.017.

Dembek, T.A., Petry-Schmelzer, J.N., Reker, P., Wirths, J., Hamacher, S., Steffen, J., Dafsari, H.S., Hövels, M., Fink, G.R., Visser-Vandewalle, V., Barbe, M.T., 2020. PSA and VIM DBS efficiency in essential tremor depends on distance to the dentatorubrothalamic tract. NeuroImage. Clin. 26, 102235 https://doi.org/10.1016/j.nicl.2020.102235.

Deuschl, G., Bain, P., Brin, M., 1998. Consensus statement of the Movement Disorder Society on Tremor. Ad Hoc Scientific Committee. Movement Disorders 13 (Suppl 3), 2–23. https://doi.org/10.1002/mds.870131303.

Ewert, S., Plettig, P., Li, N., Chakravarty, M.M., Collins, D.L., Herrington, T.M., Kühn, A. A., Horn, A., 2018. Toward defining deep brain stimulation targets in MNI space: a subcortical atlas based on multimodal MRI, histology and structural connectivity. NeuroImage 170, 271–282. https://doi.org/10.1016/j.neuroimage.2017.05.015.

Fahn, S., Tolosa, E., Marín, C., 1993. Clinical rating scale for tremor. Parkinson's Dis. Movement Disorders 2, 271–280.

Fiechter, M., Nowacki, A., Oertel, M.F., Fichtner, J., Debove, I., Lachenmayer, M.L., Wiest, R., Bassetti, C.L., Raabe, A., Kaelin-Lang, A., Schüpbach, M.W., Pollo, C., 2017. Deep brain stimulation for tremor: is there a common structure? Stereotact. Funct. Neurosurg. 95, 243–250. https://doi.org/10.1159/000478270.

Fytagoridis, A., Åström, M., Wårdell, K., Blomstedt, P., 2013. Stimulation-induced side effects in the posterior subthalamic area: distribution, characteristics and visualization. Clin. Neurol. Neurosurg. 115, 65–71. https://doi.org/10.1016/j.clineuro.2012.04.015.

Gallay, M.N., Jeanmonod, D., Liu, J., Morel, A., 2008. Human pallidothalamic and cerebellothalamic tracts: anatomical basis for functional stereotactic neurosurgery. Brain Struct. Funct. 212, 443–463. https://doi.org/10.1007/s00429-007-0170-0.

Genovese, C.R., Lazar, N.A., Nichols, T., 2002. Thresholding of statistical maps in functional neuroimaging using the false discovery rate. NeuroImage 15, 870–878. https://doi.org/10.1006/nimg.2001.1037.

Hellerbach, A., Dembek, T.A., Hoevels, M., Holz, J.A., Gierich, A., Luyken, K., Barbe, M. T., Wirths, J., Visser-Vandewalle, V., Treuer, H., 2018. DiODe: directional orientation detection of segmented deep brain stimulation leads: a sequential algorithm based on CT imaging. Stereotact. Funct. Neurosurg. 96, 335–341.

Horn, A., Li, N., Dembek, T.A., Kappel, A., Boulay, C., Ewert, S., Tietze, A., Husch, A., Perera, T., Neumann, W.-J., Reisert, M., Si, H., Oostenveld, R., Rorden, C., Yeh, F.-C., Fang, Q., Herrington, T.M., Vorwerk, J., Kühn, A.A., 2019. Lead-DBS v2: towards a comprehensive pipeline for deep brain stimulation imaging. NeuroImage 184, 293–316. https://doi.org/10.1016/j.neuroimage.2018.08.068.

Husch, A., Petersen, V.M., Gemmar, P., Goncalves, J., Hertel, F., 2018. PaCER - a fully automated method for electrode trajectory and contact reconstruction in deep brain stimulation. NeuroImage. Clin. 17, 80–89. https://doi.org/10.1016/j.nicl.2017.10.004.

Kitagawa, M., Murata, J., Kikuchi, S., Sawamura, Y., Saito, H., Sasaki, H., Tashiro, K., 2000. Deep brain stimulation of subthalamic area for severe proximal tremor. Neurology 55, 114–116. https://doi.org/10.1212/wnl.55.1.114.

Kolmac, C.I., Power, B.D., Mitrofanis, J., 1998. Patterns of connections between zona incerta and brainstem in rats. J. Comp. Neurol. 396, 544–555. https://doi.org/10.1002/(sici)1096-9861(19980713)396:4<544:aid-cne10>3.0.co;2-g.

Krauth, A., Blanc, R., Poveda, A., Jeanmonod, D., Morel, A., Székely, G., 2010. A mean three-dimensional atlas of the human thalamus: generation from multiple histological data. NeuroImage 49, 2053–2062. https://doi.org/10.1016/j.neuroimage.2009.10.042.

Limousin, P., Speelman, J.D., Gielen, F., Janssens, M., 1999. Multicentre European study of thalamic stimulation in parkinsonian and essential tremor. J. Neurol. Neurosurg. Psychiatry 66, 289–296. https://doi.org/10.1136/jnnp.66.3.289.

Lozano, A.M., 2000. Vim Thalamic Stimulation for Tremor. Arch. Med. Res. 31, 266–269. https://doi.org/10.1016/S0188-4409(00)00081-3.

Macchi, G., Jones, E.G., 1997. Toward an agreement on terminology of nuclear and subnuclear divisions of the motor thalamus. J. Neurosurg. 86, 670–685. https://doi.org/10.3171/jns.1997.86.4.0670.

Mai, J.K., Majtanik, M., 2019. Toward a common terminology for the thalamus. Front. Neuroanat. 12 https://doi.org/10.3389/fnana.2018.00114.

Meidahl, A.C., Tinkhauser, G., Herz, D.M., Cagnan, H., Debarros, J., Brown, P., 2017. Adaptive deep brain stimulation for movement disorders: the long road to clinical therapy. Movement Disorders 32, 810–819. https://doi.org/10.1002/mds.27022.

Mitrofanis, J., Mikuletic, L., 1999. Organisation of the cortical projection to the zona incerta of the thalamus. J. Comp. Neurol. 412, 173–185.

Murata, J.-I., Kitagawa, M., Uesugi, H., Saito, H., Iwasaki, Y., Kikuchi, S., Tashiro, K., Sawamura, Y., 2003. Electrical stimulation of the posterior subthalamic area for the treatment of intractable proximal tremor. J. Neurosurg. 99, 708–715. https://doi.org/10.3171/jns.2003.99.4.0708.

Nguyen, T.A.K., Djilas, M., Nowacki, A., Mercanzini, A., Schüpbach, M., Renaud, P., Pollo, C., 2019a. Analysis of patient-specific stimulation with segmented leads in the subthalamic nucleus. PLoS One 14, e0217985. https://doi.org/10.1371/journal.pone.0217985.

Nguyen, T.A.K., Nowacki, A., Debove, I., Petermann, K., Tinkhauser, G., Wiest, R., Schüpbach, M., Krack, P., Pollo, C., 2019b. Directional stimulation of subthalamic nucleus sweet spot predicts clinical efficacy: Proof of concept. Brain Stimul. 12, 1127–1134. https://doi.org/10.1016/j.brs.2019.05.001.

Nowacki, A., Debove, I., Rossi, F., Schlaeppi, J.A., Petermann, K., Wiest, R., Schüpbach, M., Pollo, C., 2018a. Targeting the posterior subthalamic area for essential tremor: proposal for MRI-based anatomical landmarks. J. Neurosurg. 1–8 https://doi.org/10.3171/2018.4.JNS18373.

Nowacki, A., Nguyen, T.A.-K., Tinkhauser, G., Petermann, K., Debove, I., Wiest, R., Pollo, C., 2018b. Accuracy of different three-dimensional subcortical human brain atlases for DBS -lead localisation. NeuroImage. Clin. 20, 868–874. https://doi.org/10.1016/j.nicl.2018.09.030.

Nowacki, A., Schlaier, J., Debove, I., Pollo, C., 2018c. Validation of diffusion tensor imaging tractography to visualize the dentatorubrothalamic tract for surgical planning. J. Neurosurg. 130, 99–108. https://doi.org/10.3171/2017.9.JNS171321.

Oostenveld, R., Fries, P., Maris, E., Schoffelen, J.-M., 2011. FieldTrip: open source software for advanced analysis of MEG, EEG, and invasive electrophysiological data. Comput. Intelligence Neurosci. 2011, 156869 https://doi.org/10.1155/2011/156869.

Petersen, M.V., Mlakar, J., Haber, S.N., Parent, M., Smith, Y., Strick, P.L., Griswold, M.A., McIntyre, C.C., 2019. Holographic reconstruction of axonal pathways in the human brain. Neuron 104, 1056–1064.e3. https://doi.org/10.1016/j.neuron.2019.09.030.

Plaha, P., Khan, S., Gill, S.S., 2008. Bilateral stimulation of the caudal zona incerta nucleus for tremor control. J. Neurol. Neurosurg. Psychiatry 79, 504–513. https://doi.org/10.1136/jnnp.2006.112334.

Power, B.D., Kolmac, C.I., Mitrofanis, J., 1999. Evidence for a large projection from the zona incerta to the dorsal thalamus. J. Comp. Neurol. 404, 554–565.

Rebelo, P., Green, A.L., Aziz, T.Z., Kent, A., Schafer, D., Venkatesan, L., Cheeran, B., 2018. Thalamic directional deep brain stimulation for tremor: spend less, get more. Brain Stimul. 11, 600–606. https://doi.org/10.1016/j.brs.2017.12.015.

Reinacher, P.C., Krüger, M.T., Coenen, V.A., Shah, M., Roelz, R., Jenkner, C., Egger, K., 2017. Determining the orientation of directional deep brain stimulation electrodes using 3D rotational fluoroscopy. AJNR Am. J. Neuroradiol. 38, 1111–1116. https://doi.org/10.3174/ajnr.A5153.

Sakai, S.T., Inase, M., Tanji, J., 1996. Comparison of cerebellothalamic and pallidothalamic projections in the monkey (Macaca fuscata): a double anterograde labeling study. The Journal of comparative neurology 368, 215–228. DOI:10.1002/(SICI)1096-9861(19960429)368:2<215:AID-CNE4>3.0.CO;2-6.

Sammartino, F., Krishna, V., King, N.K.K., Lozano, A.M., Schwartz, M.L., Huang, Y., Hodaie, M., 2016. Tractography-based ventral intermediate nucleus targeting: novel methodology and intraoperative validation. Movement Disorders 31, 1217–1225. https://doi.org/10.1002/mds.26633.

Schlaier, J., Anthofer, J., Steib, K., Fellner, C., Rothenfusser, E., Brawanski, A., Lange, M., 2015. Deep brain stimulation for essential tremor: targeting the dentato-rubro-thalamic tract? Neuromodulation 18, 105–112. https://doi.org/10.1111/ner.12238.

Schönecker, T., Kupsch, A., Kühn, A.A., Schneider, G.-H., Hoffmann, K.-T., 2009. Automated optimization of subcortical cerebral MR imaging-atlas coregistration for improved postoperative electrode localization in deep brain stimulation. AJNR. Am. J. Neuroradiol. 30, 1914–1921. https://doi.org/10.3174/ajnr.A1741.

Steigerwald, F., Müller, L., Johannes, S., Matthies, C., Volkmann, J., 2016. Directional deep brain stimulation of the subthalamic nucleus: a pilot study using a novel neurostimulation device. Movement Disorders 31, 1240–1243. https://doi.org/10.1002/mds.26669.

Steigerwald, F., Matthies, C., Volkmann, J., 2019. Directional deep brain stimulation. Neurotherapeutics 16, 100–104. https://doi.org/10.1007/s13311-018-0667-7.

Tuch, D.S., 2004. Q-ball imaging. Magn. Resonance Med. 52, 1358–1372. https://doi.org/10.1002/mrm.20279.

Tuch, D.S., Reese, T.G., Wiegell, M.R., van Wedeen, J., 2003. Diffusion MRI of complex neural architecture. Neuron 40, 885–895. https://doi.org/10.1016/S0896-6273(03)00758-X.

Vorwerk, J., Oostenveld, R., Piastra, M.C., Magyari, L., Wolters, C.H., 2018. The FieldTrip-SimBio pipeline for EEG forward solutions. Biomed. Eng. Online 17, 37. https://doi.org/10.1186/s12938-018-0463-y.

Yeh, F.-C., van Wedeen, J., Tseng, W.-Y.I., 2010. Generalized q-sampling imaging. IEEE Trans. Med. Imaging 29, 1626–1635. https://doi.org/10.1109/TMI.2010.2045126.

Yeh, F.-C., Liu, L., Hitchens, T.K., Wu, Y.L., 2017. Mapping immune cell infiltration using restricted diffusion MRI. Magn. Reson. Med. 77, 603–612. https://doi.org/10.1002/mrm.26143.